ENCIT 2018

ABCM Associação Brasileira de Engenharia e Ciências Mecânicas

17th Brazilian Congress of Thermal Sciences and Engineering
November 25th-28th, 2018, Águas de Lindóia, SP, Brazil

ENCIT-2018-0583
COMPUTATIONAL SIMULATION OF PARTICULATE FLOW AIMING THE PLUGGING OF DRILLING WELLS FRACTURES

Pedro Leineker Ochoski Machado
Luiz Eduardo Melo Lima
Marcos Vinicius Barbosa
Federal University of Technology – Paraná, Academic Department of Mechanics
Monteiro Lobato Avenue, km 4, Jardim Carvalho, 84016-210, Ponta Grossa, Paraná, Brazil
pedmac@alunos.utfpr.edu.br, lelima@utfpr.edu.br, mvbarbosa@utfpr.edu.br

Abstract. *In the drilling industry, the lost circulation phenomenon defined as the drilling fluid invasion into the substrate leads to a cost increase and productive time decrease. When fractures are present in the substrate, such a phenomenon can be intensified favoring the fluid loss. One of the methods applied to correct the lost circulation associated with the presence of fractures is to add particulate material to the drilling fluid, aiming the total or partial plugging of the fractures. The objective of this study is to perform a coupling test between DDPM-DEM methods on the fracture plugging problem, which includes velocity measurement of a settling sphere and the collision of a single particle with a static wall, by using of the Ansys/Fluent® commercial software for Computational Fluid Dynamics (CFD). An Eulerian approach to the fluid and a Lagrangian one to the particles is applied through the Dense Discrete Phase Model (DDPM), taking accounting the collisions between the particles through the Discrete Element Method (DEM). The numerical results are compared with experimental data available in the literature and major findings are discussed.*

Keywords: *computational simulation, numerical analysis, fracture plugging.*

1. INTRODUCTION

The process of drilling oil wells generally occurs in a rotating way, where the weight and rotation of the drill bit present in the drilling column will be responsible for accessing the formation. De Lai (2013) says that the region contained between the rock formation wall and the drill column is called the annular space, space through which the drilling fluid injected into the drilling column returns to the surface, carrying with it the rock fragments from the drilling.

Crespo *et al.* (2012) affirm that wellbore hydraulics are receiving increased attention in the past few years due to its several drilling challenges. According to Adachi *et al.* (2004), wellbore stability during drilling can be linked with fracture occurrence, that may by originate basically in two ways: pre-existing fractures in the rock that propagate during the drilling, or the interaction between the drill bit and formation, which generates high-pressure gradients in the wellbore and causes rock fracture.

Due to this fact, Crespo *et al.* (2012) state that it is extremely important to quantitatively characterize the pressure limits of the drilling well, since the operation outside this pressure limit range can cause several problems, among them, the presence of fractures in the rock formation. A scheme of a drilling well containing fractures can be seen in Fig. 1.

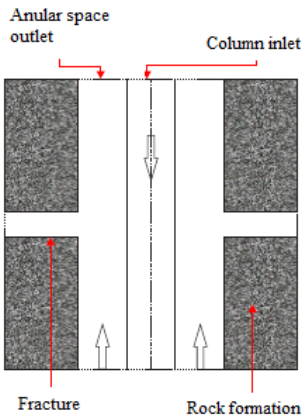

Figure 1. Simplified geometry of a wellbore; adapted from Barbosa (2015).

Crespo *et al.* (2012) add that in addition to the presence of fractures in the drilling well operate above the pressure limit (also called surge pressure) leads to the occurrence of fluid leakage through fractures and also to the rock formation porosity. As a result, the level of drilling fluid decreases and consequently the hydrostatic pressure of the drilling well is reduced, causing formation fluids to enter the drilling well. This also occurs when working below the pressure limit (also called swab pressure), making that one of the main reasons for explosions in drilling wells.

In addition to the effects of the lost circulation evidenced by Crespo *et al.* (2012), Datwani (2012) add that as the amount of drilling fluid is reduced, it may not be enough to perform the drilling efficiently, which can result in damage to the well and the drill bit. That phenomenon is called dry drilling. Thus, both by fluid lost and damaged tools, the lost circulation leads to high additional costs to the process of drilling wells.

Alexander (1989) adds that the maximum amount of drilling mud lost tolerated is approximately one barrel per hour, in a way that corrective measures are needed for a greater amount of drilling mud lost, and drilling is not resumed until the fracture is plugged.

Still, according to Alexander (1989), the perfect case for drilling oil wells corresponds to a case where mud lost will not occur, but sometimes, even correct drilling techniques cannot prevent the lost circulation phenomenon. Consequently, that phenomenon needs special attention so it can be corrected or prevented to avoid additional costs.

Due to this fact, Alexander (1989) affirms that many methods have been tested to pursuit the plugging of drilling wells fractures, such as increasing the viscosity of the drilling mud or the resistance of the mud to drain into fractures. Also, a wide variety of materials have been added to the drilling mud in an attempt to the fracture plugging.

According to Whitfill and Hemphill (2004), Gockel (1984), and Gatlin and Nemir (1961), one of the ways to overcome the lost circulation problem is the particles injection with specific granulometry in the drilling column. Such particles would be charged by the drilling fluid and, upon returning to the surface of the annular space and reaching the region containing a fracture, would begin to deposit within the fracture, filling it in the future. The proposed study uses such an approach to carry out an analysis of fracture plugging through the particles injection.

The objective of this study is to perform a coupling test between DDPM-DEM methods on the fracture plugging problem, which includes velocity measurement of a settling sphere and the collision of a single particle with a static wall, by using of the Ansys/Fluent® commercial software for Computational Fluid Dynamics (CFD). An Eulerian approach to the fluid and a Lagrangian one to the particles is applied through the Dense Discrete Phase Model (DDPM), introduced by Popoff and Braun (2007), taking accounting the collisions between the particles through the Discrete Element Method (DEM), introduced by Cundall and Strack (1979).

2. METHODOLOGY

The mathematical formulation is based on two equations set: one for the continuous phase (fluid) and another for the dispersed one (particles). For simplification, the fluid is assumed Newtonian with constant properties, for an isothermal and incompressible flow. The equations for the continuous phase are the mass conservation and the Navier-Stokes, as can be seen in Eqs. (1) and (2), respectively (Ansys, 2012):

$$\frac{\partial(\varepsilon_\beta \rho_\beta)}{\partial t} + \nabla \cdot (\varepsilon_\beta \rho_\beta \boldsymbol{u}_\beta) = 0 \tag{1}$$

$$\frac{\partial(\varepsilon_\beta \rho_\beta \boldsymbol{u}_\beta)}{\partial t} + \nabla \cdot (\varepsilon_\beta \rho_\beta \boldsymbol{u}_\beta \boldsymbol{u}_\beta) = -\varepsilon_\beta \nabla p_\beta + \nabla(\varepsilon_\beta \mu_\beta \nabla \cdot \boldsymbol{u}_\beta) + \varepsilon_\beta \rho_\beta \boldsymbol{g} + \boldsymbol{F}_{DPM} + \boldsymbol{S}_{DPM} \tag{2}$$

where ε_β represents the volume fraction of the continuous phase, t is the time, the velocity vector is given by $\boldsymbol{u}_\beta$, ρ_β is the continuous phase density, p_β is the pressure distribution and $\boldsymbol{g}$ represents the gravity acceleration vector. $\boldsymbol{S}_{DPM}$ is the source term due to the fluid displacement in relation to the particles entry in a given control volume and $\boldsymbol{F}_{DPM}$ regards to the coupling between the phases.

Concerning the particles (dispersed phase), the velocity is defined in terms of Newton's second law of motion, as can be seen in Eq. (3), while the position is represented in Eq. (4):

$$m_p \frac{\mathrm{d}\boldsymbol{u}_p}{\mathrm{d}t} = \boldsymbol{F}_d + \boldsymbol{F}_{gb} + \boldsymbol{F}_{pg} + \boldsymbol{F}_{vm} + \boldsymbol{F}_{lv} + \boldsymbol{F}_{DEM} \tag{3}$$

$$\frac{\mathrm{d}\boldsymbol{x}_p}{\mathrm{d}t} = \boldsymbol{u}_p \tag{4}$$

where the particle mass is given by m_p, $\boldsymbol{F}_d$ is the drag force, $\boldsymbol{F}_{gb}$ is the counterbalance between the gravity and buoyancy forces, $\boldsymbol{F}_{pg}$ represents the pressure gradient force, $\boldsymbol{F}_{vm}$ is the virtual mass force, $\boldsymbol{F}_{lv}$ is the Saffman's lift force, $\boldsymbol{F}_{DEM}$ symbolizes the force related to the particles collisions and the particle velocity and position are represented by $\boldsymbol{u}_p$ and $\boldsymbol{x}_p$, respectively.

The expressions to evaluate all those forces can be seen in Tab. 1 where ρ_p is the particle density, C_d is the drag coefficient between the particle and the fluid, Re_p is the particle's Reynolds number, given by $\mathrm{Re}_p = \rho_\beta |\boldsymbol{u}_\beta - \boldsymbol{u}_p| d_p / \mu_\beta$. C_{ls} is the Saffman lift constant (Li and Ahmadi, 1992) and C_{vm} is the virtual mass coefficient (Kendoush *et al.*, 2007).

Table 1. Expressions to evaluate the acting forces.

Force	Equation
Gravitational and buoyancy forces	$\boldsymbol{F}_{gb} = m_p \frac{\rho_p - \rho_\beta}{\rho_p} \boldsymbol{g}$
Drag force	$\boldsymbol{F}_d = \frac{3}{4} \frac{m_p \mu_\beta}{\rho_p d_p^2} C_d \mathrm{Re}_p (\boldsymbol{u}_\beta - \boldsymbol{u}_p)$
Saffman's lift force	$\boldsymbol{F}_{ls} = C_{ls} m_p \frac{\rho_\beta}{\rho_p} (\nabla \times \boldsymbol{u}_\beta) \times (\boldsymbol{u}_\beta - \boldsymbol{u}_p)$
Virtual mass force	$\boldsymbol{F}_{vm} = C_{vm} m_p \frac{\rho_\beta}{\rho_p} \frac{D}{Dt} (\boldsymbol{u}_\beta - \boldsymbol{u}_p)$
Pressure gradient force	$\boldsymbol{F}_{pg} = m_p \frac{\rho_\beta}{\rho_p} (\boldsymbol{u}_\beta \nabla \cdot \boldsymbol{u}_p)$

The collision force, $\boldsymbol{F}_{DEM}$, is a combination of the normal and tangential forces generated by the particle collisions:

$$\boldsymbol{F}_{DEM} = \boldsymbol{F}_t + \boldsymbol{F}_n \tag{5}$$

The normal force is calculated through a spring-dashpot model (Luding, 1998), as shown in Eq. (6):

$$\boldsymbol{F}_n = [k\delta + \gamma(\boldsymbol{u}_{12} \cdot \boldsymbol{\lambda}_{12})]\boldsymbol{\lambda}_{12} \tag{6}$$

where k, δ, γ, u_{12} and $\boldsymbol{\lambda}_{12}$ are respectively, the spring constant, the overlap between the particles, the damping coefficient, the relative velocity and the normal direction of the collision. The damping coefficient is calculated using Eq. (7) in which m_{12} represents the reduced mass and t_{col} is the collision time.

$$\gamma = -2\frac{m_{12}}{t_{col}} \ln \eta \tag{7}$$

The tangential force $\boldsymbol{F}_t$ is calculated using a Coulomb model as represented in Eq. (8):

$$\boldsymbol{F}_t = -\mu_a |\boldsymbol{F}_n| \xi_{12} \tag{8}$$

where μ_a is the friction coefficient and ξ_{12} is the tangential direction.

3. VERIFICATION PROBLEMS

This section presents four verifications analysis: terminal velocity, fully developed flow, collision, and injection test.

3.1 Fully developed flow

An important hypothesis that must be taken into account is that at the moment the particles reach the fractured region, the fluid is in a fully developed flow, so it is necessary to verify if the flow profile obtained by simulation matches the profile obtained analytically.

For that, a fluid (water) present between two vertically oriented flat walls (in position y) flowing in the opposite direction from gravity was simulated, and the velocity profile obtained was compared with a profile resulting from the simplification of the conservation equation of linear momentum in the Y direction, obtaining Eq. (9):

$$v = \frac{h^2}{2\mu} \left\{ \left[\left(\frac{\mathrm{d}P}{\mathrm{d}y} \right) + \rho_\beta g \right] \left[\left(\frac{x}{h} \right)^2 - \frac{1}{4} \right] \right\} \tag{9}$$

where the position and the fluid velocity are represented by x and v respectively. The fluid density and dynamic viscosity are given by ρ_β and μ respectively. Gravity is represented by g, the geometry dimension is given by h, and $(\mathrm{d}P/\mathrm{d}y)$ represents the pressure gradient in the Y direction.

To perform the simulation, a geometry with $h = 0.12$ m was used. Since the only simulation input consists of the fluid velocity inlet and not the pressure gradient when the flow pressure gradient is obtained by the software, it already performs a forces balance and includes the gravity influence, so Eq. (9) is rewritten as Eq. (10):

$$v = \frac{h^2}{2\mu} \left(\frac{\mathrm{d}P'}{\mathrm{d}y} \right) \left[\left(\frac{x}{h} \right)^2 - \frac{1}{4} \right] \tag{10}$$

The comparison of the profile obtained through simulation with that obtained by Eq. (10) can be observed in Fig. 2. The data obtained by the simulation are presented in a coherent way with the data obtained by the conservation equation of linear momentum, ensuring that it is possible to perform the particles injection in a fully developed fluid.

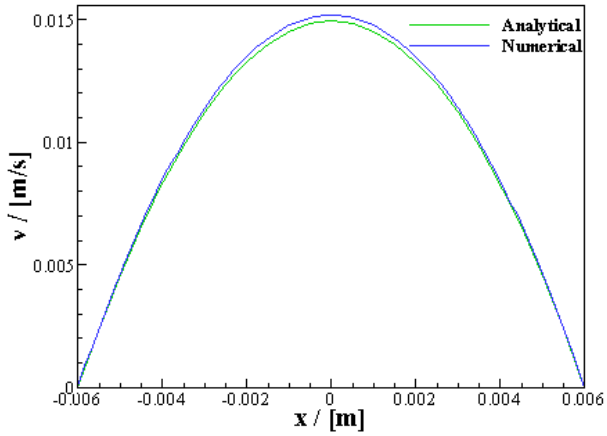

Figure 2. Numerical and analytical velocity profile.

3.2 Terminal velocity

In order to verify the behavior of an injected spherical particle in a resting fluid, the terminal velocity test was performed, which consists of leaving a particle with defined properties (density, diameter, and zero initial velocity) in a fluid also with known properties (density and dynamic viscosity) that is at rest. After the injection, the behavior of the particle velocity who has its movement initiated due to the gravity action was verified until it reaches its terminal speed value.

Two fronts were used as a reference to verify if the terminal velocity value obtained numerically corresponds to the actual value. For that, experimental results provided by Mordant and Pinton (2000), and also values obtained analytically through a forces balance were used.

In order to compare the simulation data with the data obtained by Mordant and Pinton (2000), a sphere with a diameter of 5×10^{-4} m and a density of 2560 kg/m^3 was left in a container consisting of water at room temperature, with density of 998.1 kg/m^3 and dynamic viscosity equal to 0.001003 Pa.s. Willing to perform a mesh test and also verify the time step influence on the simulation, three distinct meshes were constructed with cubic volume controls (VC) of dimensions equal to a diameter, a diameter and a half, and two particle diameters, using three different time steps, 10^{-3}, 10^{-4} and 10^{-5} seconds, totaling nine different simulations. The results obtained in the simulations and their comparison with the results of Mordant and Pinton (2000) can be observed in Tab. 2:

Table 2. Relative difference (RD) between terminal velocity values of a settling sphere obtained by the numerical method and experimental data given by Mordant and Pinton (2000).

Case	VC dimension / [m]	Time step size / [s]	Terminal velocity / [m/s]		RD / [%]
			Numerical	Experimental	
A	0.0005	10^{-3}	0.0781	0.0741	5.43
B	0.0005	10^{-4}	0.0755		4.57
C	0.0005	10^{-5}	0.0749		1.03
D	0.00075	10^{-3}	0.0779		5.10
E	0.00075	10^{-4}	0.0765		3.28
F	0.00075	10^{-5}	0.0760		2.54
G	0.001	10^{-3}	0.0775		4.61
H	0.001	10^{-4}	0.0770		3.91
I	0.001	10^{-5}	0.0761		2.72

From Tab. 2 it can be verified that the best scenario of the numerical results compared to the experimental method (Mordant and Pinton, 2000) was obtained with case C, indicating that the combination of a VC with a dimension of one diameter and a time step size of 10^{-5} seconds is the best among all others tested. In order to verify the behavior of the particle velocity until it reaches the terminal velocity value, the non-dimensional velocity profiles were also graphically compared for all cases, as can be seen in Figs. 3, 4, and 5.

Figures 3, 4, and 5 show that regardless of the time step size or VC dimension, non-dimensional terminal velocity behaves in a very similar way to the results obtained by Mordant and Pinton (2000), having it's biggest difference on the acceleration stage, which according to Barbosa *et al.* (2015) may arise from the difficulties involved in measuring the velocity of such a small particle. Therefore, the DDPM model presents satisfactory results on the terminal velocity of a settling sphere.

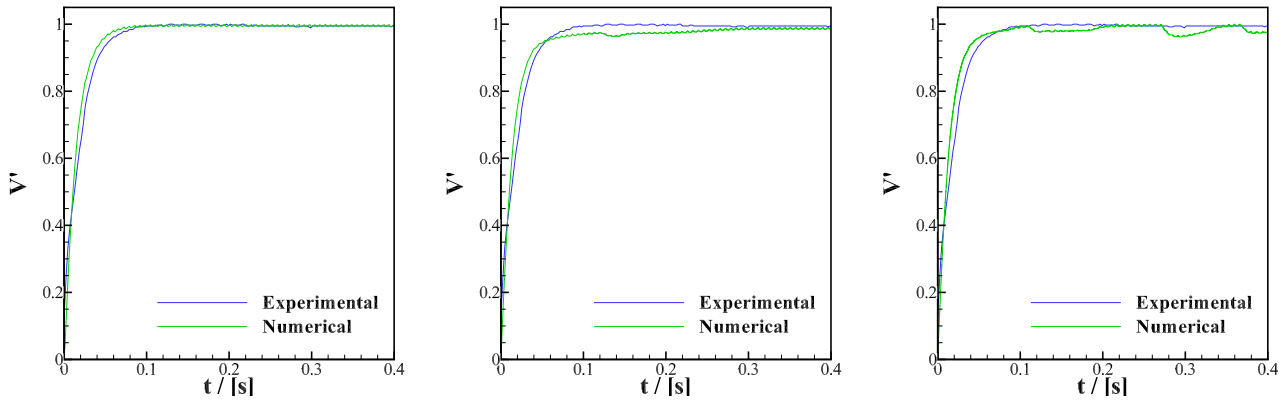

(a) (b) (c)

Figure 3. Particle non-dimensional velocity for each time step size considering the cubic volume of 5×10^{-4} m, according to Tab. 2: (a) Case A - 10^{-3} s; (b) Case B - 10^{-4} s; (c) Case C - 10^{-5} s.

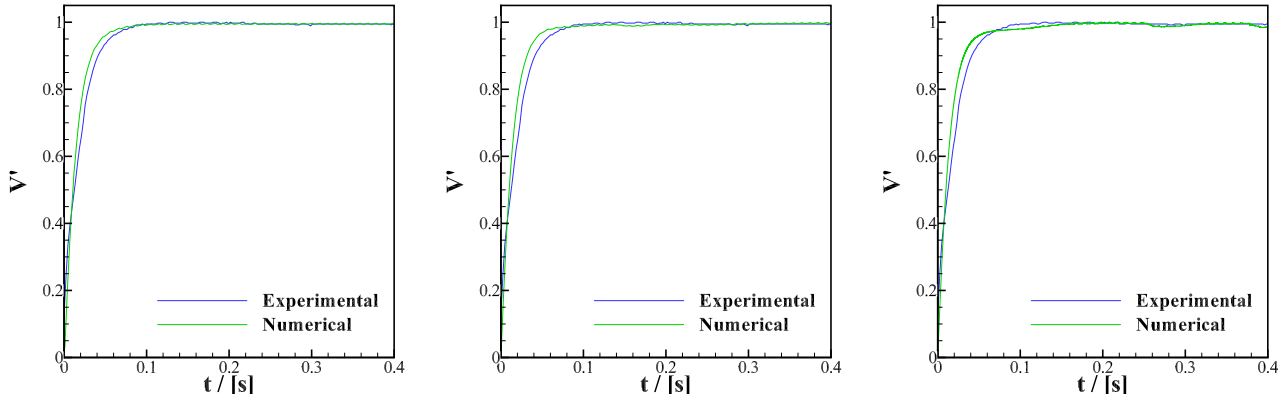

(a) (b) (c)

Figure 4. Particle non-dimensional velocity for each time step size considering the cubic volume of 7.5×10^{-4} m, according to Tab. 2: (a) Case D - 10^{-3} s; (b) Case E - 10^{-4} s; (c) Case F - 10^{-5} s.

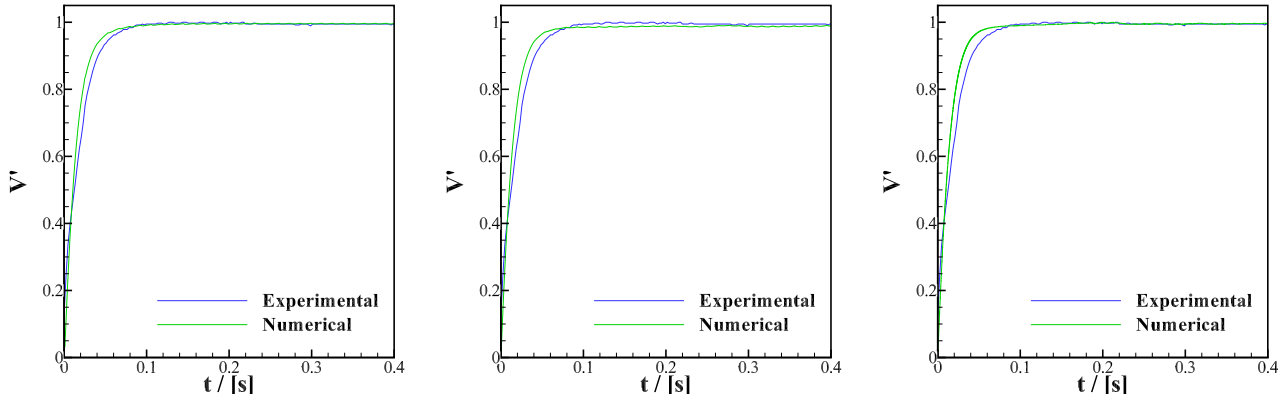

(a) (b) (c)

Figure 5. Particle non-dimensional velocity for each time step size considering the cubic volume of 1×10^{-3} m, according to Tab. 2: (a) Case G - 10^{-3} s; (b) Case H - 10^{-4} s; (c) Case I - 10^{-5} s.

For the comparison of the numerical results with the analytical ones, a force balance was performed around the particle, considering that, after some simplifications, the particle weight strength would correspond to the sum of the drag force with the thrust force, situation that corresponds to the moment when the particle would be flowing with its terminal velocity. Thus, it has been determined that the particle terminal velocity can be determined according to Eq. (11):

$$V_t = \sqrt{\frac{2\mho g}{C_d A} \frac{(\rho_p - \rho_\beta)}{\rho_\beta}} \tag{11}$$

where the particle terminal velocity is represented by V_t, the fluid and particle densities are expressed by ρ_β and ρ_p respectively. The particle volume is given by $\mho$, g is the gravity acceleration, C_d is the drag coefficient between the particle and the fluid, and the particle area is given by A.

The drag coefficient model provided by Kelessidis (2003) was used for the drag coefficient. Eq. (12) was used for the Re range provided by Mordant and Pinton (2000):

$$\log(C_d \mathrm{Re}/24 - 1) = 0.6305 \log \mathrm{Re} - 0.713 \tag{12}$$

where the Reynolds number for the flow and the drag coefficient of the settling sphere are given by Re and C_d.

The results obtained by the comparison with the analytical method can be observed in Tab. 3.

Table 3. Relative difference (RD) between terminal velocity values of a settling sphere obtained by numerical and analytical methods.

Case	Terminal velocity / [m/s]		RD / [%]
	Numerical	Analitycal	
A	0.0781	0.0763	2.45
B	0.0755		1.61
C	0.0749		1.83
D	0.0779		2.14
E	0.0765		0.36
F	0.0760		0.35
G	0.0775		1.65
H	0.0770		0.98
I	0.0761		0.18

It is verified that the values obtained in a numerical way approach satisfactorily to the values obtained both experimentally and analytically, occurring variations due to different models and simplifications used.

Knowing that the best scenario to obtain terminal velocity numerically corresponds to Case C, another test has been performed with a sphere with a diameter of 8×10^{-4} m and a density of 7710 kg/m^3. The results can be observed in Fig. 6 and it can be seen that for a sphere with different a diameter than the one used for Cases A-I, the numerical approach also obtain satisfactory results for the terminal velocity, showing that DDPM can be used to study that problem.

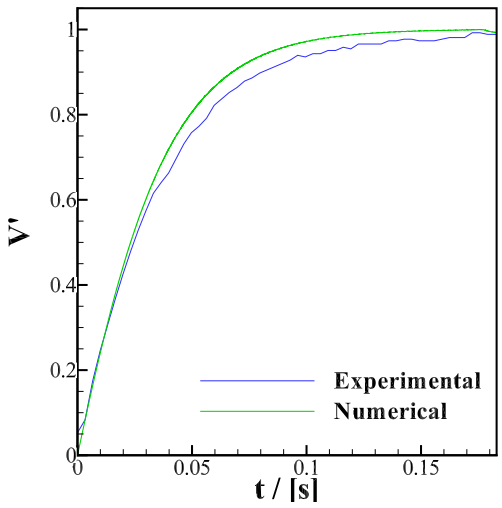

Figure 6. Non-dimensional velocity of a sphere with a diameter of 8×10^{-4} m and a density of 7710 kg/m^3.

3.3 Collision test

In order to perform the collision test, a particle with no initial velocity is dropped in a steady fluid, then starts to accelerate until it reaches it's terminal velocity and then collides with a static wall.

This test was based on an experimental carried out by Gondret *et al.* (2002), where a 3 mm steel sphere (density of 7800 kg/m^3) is dropped in Silicone oil RV10 (density of 935 kg/m^3 and viscosity of 10×10^{-3} Pa.s) contained in an rectangular vessel (10 cm $\times$ 10 cm $\times$ 30 cm).

Gondret *et al.* (2002) affirm that "the velocity decreases nonlinearly with time and the velocity at the end of a rebound is significantly smaller than at the beginning", therefore, knowing that the restitution coefficient decreases with decreasing impact velocity, a different restitution coefficient was set for each bounce of the sphere, being of 0.78 for the first collision, and then of 0.66, 0.45, 0.25, and 0 for the successive collisions.

After the test was performed, a comparison was made between data obtained by Gondret *et al.* (2002) and numerically with Ansys/Fluent®, as it can be seen in Fig. 7.

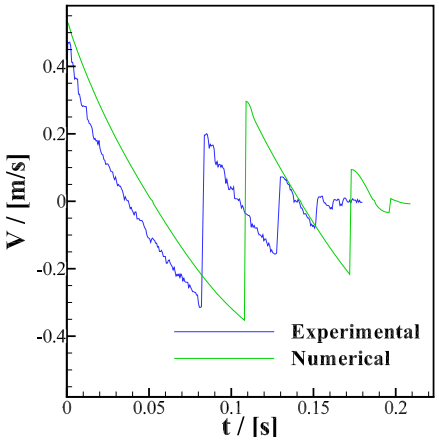

Figure 7. Particle velocity after each bounce.

Figure 7 shows that the sphere stops after the same amount of bounces in both cases, although there's a difference in the velocity magnitude after each bounce and also the time that each one occurred. Even with such a difference, it is considered that the numerical result is satisfactory since the greatest time and velocity difference is approximately 0.05 s and 0.05 m/s. This indicates that the DDPM-DEM model is also satisfactory to evaluate the wet collisions.

3.4 Injection test

With the terminal velocity, fluid development, and collision tests performed, the fracture filling process can be simulated. For this, using the symmetry shown in Fig. 1, a geometry was constructed referring to the half of a wellbore, as can be observed in Fig. 8.

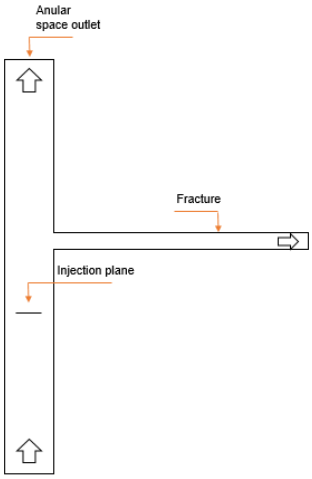

Figure 8. Particle injection simulation's geometry.

In order to correctly simulate the flow conditions of the lost circulation phenomenon, the procedure proposed by De Lai (2013) is applied. It mainly consists in setting a flow rate, based on fluid velocity, at the wellbore inlet region and the desired fluid loss at the end of the fracture as well as the remainder of the flow rate at the wellbore outlet. Then, the simulation is conducted up to a fully developed flow and the pressure at the fracture outlet and the wellbore outlet are collected. At last, a new simulation is configured with said pressures and, when a fully developed flow is again achieved, the particle injection process begins. The parameters used for the simulation and also the parameters obtained through this can be observed in Tab. 4.

Table 4. Parameters for injection test.

Parameter	Value
Fluid density	1187.6 kg/m^3
Fluid dynamic viscosity	0.027973 kg/(m.s)
Fluid injection velocity	0.261714 m/s
Maximum flow velocity	0.391285 m/s
Pressure at fracture outlet	-264.47504 Pa
Pressure at wellbore outlet	31.126383 Pa

For the new simulation, which was set up with those pressure values as a boundary condition in its reference regions and with the particles injection with known properties (density of 2969 kg/m^3 and diameter of 5×10^{-4} m) and velocity equal to the maximum velocity obtained for the flow in the previous simulation, the results can be seen in Fig. 9.

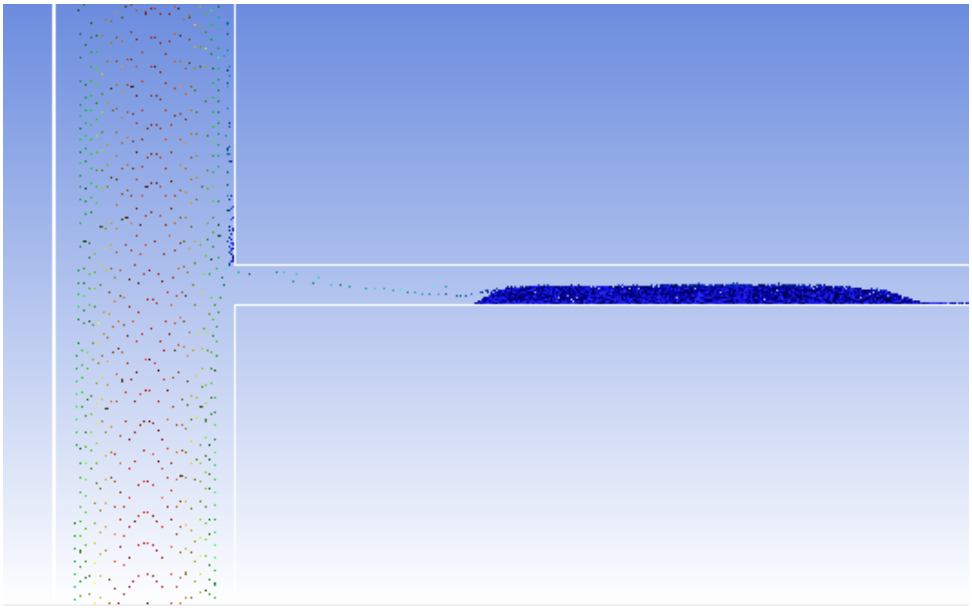

Figure 9. Particles injection and fracture plugging.

From Fig. 9 it can be seen that the particles injection occurred in the desired fashion. One can notice that the particles do deposit inside the fracture as expected. Also, it can be seen that the particles follow the fully developed flow profile of the fluid, which result was also expected as the simulation result.

The effects of the particles injection process, as well as the particle deposition inside the fracture, are analyzed by two parameters: the pressure at the wellbore inlet and the fluid loss at the end of the fracture. The pressure analysis at the wellbore inlet is presented in Fig 10.

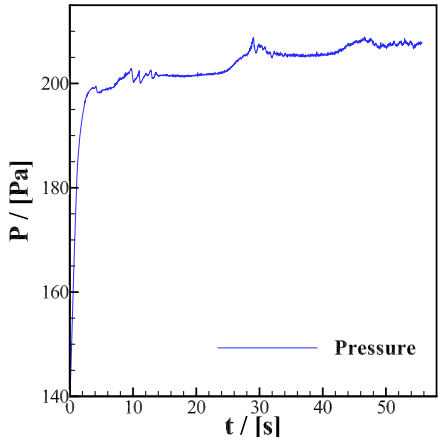

Figure 10. Pressure at wellbore inlet.

As it was expected, from Fig. 10 it can be seen that with the particles injection there is an increase in the annular space entrance pressure, which is approximately one and a half times the initial pressure value. That occurs basically due to the particles' vertical accumulation, in which their weight causes an increase in the pressure magnitude of the analyzed region.

In Fig.11. the monitoring of the fluid loss through the fracture is presented.

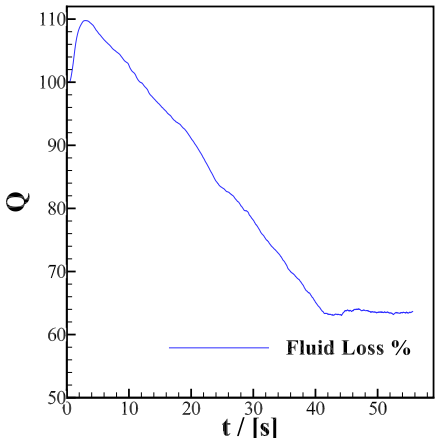

Figure 11. Fluid loss at fracture outlet.

Considering that before the particles injection, Q stands at 100%, Fig.11 shows the behavior of the fluid loss over time as a function of the initial mass flow. It can be seen that when the injection starts there is an increase in the fluid loss since the particles entrance in the geometry causes the expulsion of a fluid volume contained in the fracture of the same volume proportion of such particles (overshoot).

After that, as particles accumulate inside the fracture, the flow is gradually reduced, since these create a barrier that reduces the amount of fluid that enters the fracture and generate an increase in the pressure drop in the fracture. This occurs until a point where the pressure drop is not sufficient to promote the particles entry into the fracture, causing them to take the exit from the annular space as the preferred flow line, thereby stabilizing the mass flow at the fracture outlet.

From Fig. 11 it can be seen that with the parameters used for such simulation, a reduction of about 36.34% in the mass flow rate of fluid in the fracture was obtained, fulfilling the objective of such simulation, which proves that the coupling between DDPM-DEM methods can be used to obtain numerical results for fracture plugging.

4. CONCLUSIONS

In this work, to achieve the fracture plugging an analysis was performed on the particulate material injection problem in a fractured channel containing a Newtonian fluid. Four verification problems were analyzed: the terminal velocity, the fully developed flow, the collision, and the injection test.

All four verification problems behaved in a very similar way with the experimental and analytical data used as a reference in this study, proving that the coupling between DDPM-DEM methods allows us to obtain satisfactory results when dealing with the problems analyzed.

With all the tests performed, it is guaranteed that the numerical model used yield satisfactory results on the real phenomena, so it is now possible to carry out a new study on the parameters influence of the particles and the fluid in the fracture plugging.

5. ACKNOWLEDGMENTS

The authors thank the Federal University of Technology – Paraná for the support received for the development of this work and the participation in this event.

6. REFERENCES

Adachi, J., Bailey, L., Houwen, O.H., Meeten, G.H., Way, P.W., Growcock, F.B. and Schlemmer, R.P., 2004. "Depleted zone drilling: reducing mud losses into fractures". In *IADC/SPE Drilling Conference*. Society of Petroleum Engineers, SPE, Dallas, Texas, USA. doi:10.2118/87224-MS. URL `https://www.onepetro.org/conference-paper/SPE-87224-MS`.

Alexander, W., 1989. "Composition and method of controlling lost circulation from wellbores". URL `https://patents.google.com/patent/US4836940A/`. US Patent 4,836,940.

Ansys, 2012. *Ansys/Fluent Release Version 14.5 Manual*. Ansys Inc., Canonsburg, Pennsylvania, USA. Documentation.

Barbosa, M.V., 2015. *Análise paramétrica de escoamento particulado aplicado ao preenchimento de fraturas*. Master's Thesis, Universidade Tecnológica Federal do Paraná, Curitiba, Paraná, Brazil. URL http://repositorio.utfpr.edu.br/jspui/handle/1/1266. Mestrado em Engenharia Mecânica e de Materiais (in portuguese).

Barbosa, M.V., De Lai, F.C., Franco, A.T. and Junqueira, S.L.M., 2015. "Eulerian-Lagrangian approach applied to particulate flow using dense discrete phase model". In *Proceedings of the IV Journeys in Multiphase Flows (JEM 2015)*. Campinas, São Paulo, Brazil. ISSN 2447-2387. URL https://eventos.abcm.org.br/jem2015/PDFS/JEM-2015-0071.PDF. Paper ID: JEM2015-0071.

Crespo, F.E., Ahmed, R.M., Saasen, A., Enfis, M. and Amani, M., 2012. "Surge-and-swab pressure predictions for yield-power-law drilling fluids". *SPE Drilling & Completion*, Vol. 27, No. 4, pp. 574–585. doi:10.2118/138938-PA. URL https://www.onepetro.org/journal-paper/SPE-138938-PA.

Cundall, P.A. and Strack, O.D.L., 1979. "A discrete numerical model for granular assemblies". *Geotechnique*, Vol. 29, No. 1, pp. 47–65. doi:10.1680/geot.1979.29.1.47. URL https://www.icevirtuallibrary.com/doi/10.1680/geot.1979.29.1.47.

Datwani, A., 2012. *Review of lost circulation mechanisms with the focus on loss to natural and drilling induced fractures*. Master's Thesis, Department of Process Engineering and Applied, Dalhousie University, Halifax, Nova Scotia, Canada. Master of Engineering.

De Lai, F.C., 2013. *Simulação numérica do escoamento particulado para o preenchimento de canal fraturado*. Master's Thesis, Universidade Tecnológica Federal do Paraná, Curitiba, Paraná, Brazil. URL http://repositorio.utfpr.edu.br/jspui/handle/1/793. Mestrado em Engenharia Mecânica e de Materias (in portuguese).

Gatlin, C. and Nemir, C.E., 1961. "Some effects of size distribution on particle bridging in lost circulation and filtration tests". *Journal of Petroleum Technology*, Vol. 13, No. 6, pp. 575–578. doi:10.2118/1652-G-PA. URL https://www.onepetro.org/journal-paper/SPE-1652-G-PA.

Gockel, J., 1984. "Prevention of lost circulation of drilling muds". URL https://patents.google.com/patent/US4460052A. U.S. Patent No. 4,460,052.

Gondret, P., Lance, M. and Petit, L., 2002. "Bouncing motion of spherical particles in fluids". *Physics of Fluids*, Vol. 14, No. 2, pp. 643–652. doi:10.1063/1.1427920. URL https://aip.scitation.org/doi/10.1063/1.1427920.

Kelessidis, V.C., 2003. "Terminal velocity of solid spheres falling in Newtonian and non-Newtonian liquids". *Techn. Chron. Sci. J., Techn. Chamber Greece*, Vol. 1, p. 2.

Kendoush, A.A., Sulaymon, A.H. and Mohammed, S.A.M., 2007. "Experimental evaluation of the virtual mass of two solid spheres accelerating in fluids". *Experimental Thermal and Fluid Science*, Vol. 31, No. 7, pp. 813–823. doi:https://doi.org/10.1016/j.expthermflusci.2006.08.007. URL http://www.sciencedirect.com/science/article/pii/S0894177706001385.

Li, A. and Ahmadi, G., 1992. "Dispersion and deposition of spherical particles from point sources in a turbulent channel flow". *Aerosol Science and Technology*, Vol. 16, No. 4, pp. 209–226. doi:10.1080/02786829208959550. URL https://doi.org/10.1080/02786829208959550.

Luding, S., 1998. "Collisions & contacts between two particles". In *Physics of dry granular media*, Springer, pp. 285–304. doi:10.1007/978-94-017-2653-5_20. URL https://link.springer.com/chapter/10.1007%2F978-94-017-2653-5_20.

Mordant, N. and Pinton, J.F., 2000. "Velocity measurement of a settling sphere". *The European Physical Journal B - Condensed Matter and Complex Systems*, Vol. 18, No. 2, pp. 343–352. doi:10.1007/pl00011074. URL https://link.springer.com/article/10.1007%2FPL00011074.

Popoff, B. and Braun, M., 2007. "A Lagrangian approach to dense particulate flows". In *Proceedings of the 6th International Conference on Multiphase Flow (ICMF 2007)*. Leipzig, Germany.

Whitfill, D.L. and Hemphill, T., 2004. "Pre-treating fluids with lost circulation materials". *Drilling Contractor*, Vol. 60, No. 3, pp. 54–57.

7. RESPONSIBILITY NOTICE

The authors are the only ones responsible for the printed material included in this paper.